Catalysis Today 159 (2011) 64–73

Contents lists available at ScienceDirect

Catalysis Today

journal homepage: www.elsevier.com/locate/cattod

High-throughput syntheses of nano-scaled mixed metal sulphides

M.A. Kolb, W.F. Maier, K. Stöwe*

Technical Chemistry, Saarland University, 66123 Saarbrücken, Germany

ARTICLE INFO

Article history:
Available online 17 August 2010

Keywords:
Metal sulphides
Mixed metal sulphides
High-throughput experimentation
Nano-scaled materials
Microemulsions

ABSTRACT

The use of metal and mixed metal sulphides as heterogeneous catalysts is often hampered by an undefined composition formed by in situ sulphidation of oxides. Controlled synthesis methods are serial and thus slow, because high-throughput (HT) methods for the well-directed syntheses of exactly defined metal sulphides and especially mixed metal sulphides are still lacking. The present contribution presents the development of HT synthesis methods for a broad range of nano-scaled sulphides for various applications, such as heterogeneous catalysts or photocatalysts. The nano-scale regime for the particle sizes offers the possibilities of high surface area, appearance of quantum size effects and the possibility of modification of their properties as well as stabilisation of the particles by surface coating. Several precursor molecules have been tested, which hydrolyse under specific conditions and release sulphide ions for metal and mixed metal sulphide precipitation. Particle size confinement was achieved by w/o microemulsions using non-ionic surfactants. In a first step for the parallel synthesis of sulphides a 9-fold reactor assembly was developed, which offers the possibility of synthesis by precipitation and separation of the resulting materials by filtration in one setup.

1. Introduction

Metal sulphides are significantly less recognised in catalysis than metals or metal oxides although sulphides catalyze major industrial processes, such as hydrotreating and hydrocracking in fuel refinery [1–9]. In addition to these important processes there are a number of applications of minor relevance such as precious metal sulphides for the electrochemical reduction of O_2 and the reduction of SO_2 in the presence of NH_3 [10,11]. Further reactions catalyzed by metal sulphides are selective hydrogenation processes, oligomerisation of hydrocarbons, CO-shift reaction, and methanol synthesis from syngas [12–15]. Also of broad interest are the photocatalytic properties of metal sulphides [16].

The electronic properties of metal sulphides differ from those of metals and metal oxides and hence make them promising candidates as effective catalysts for various photocatalytic reactions. Photocatalysis research is strongly interwoven with the development of nano-materials. The reduction of the particle size to small cluster sizes is a promising approach for activity improvement and modification of electronic and, more generally, catalytic properties. Several approaches have been used in the literature for the synthesis of nano-scaled sulphides [17–30].

Combinatorial workflows are widely and successfully used for the search of new metal and metal oxide catalyst systems [31–34]. To our best knowledge, no such workflows exist for systems based on metal sulphides with particles sizes in the nano-regime. Our research objective is to develop such a workflow, starting with the development of a parallel synthesis strategy for nano-scaled mixed metal sulphides. The method needs to fulfil several requirements. It has to be applicable to a broad range of metal sulphides. Synthesis recipes broadly applicable for a wide range of metal compounds are still missing in the literature and the main focus is on zinc and cadmium sulphides [18,27]. But the workflow can only yield mixed metal sulphides in the constraints given by the chemistry of metal sulphides. A major constraint in this context is the limited solubility of the metal sulphides in each other due to structural differences. The particle sizes obtained by the method should be smaller than 10 nm in order to show quantum size effects. This requirement is dictated by the fact that only for small cluster sizes significant variations are regularly observed in the electronic structure compared to bulk materials.

The synthesised nano-sized materials need to be stabilised, because they are *per se* instable with respect to agglomeration. Stabilisation is generally achieved by surface modification. Chemically adsorbed molecules on the surface act as spacers and thus can prevent agglomeration of the nanoparticles. The modification can be realised during the synthesis of the nanoparticles (one step process) or in a separate step after the synthesis of the particles (two step process). The surface modification may not only prevent agglomeration, but additionally give the compound unique properties such

* Corresponding author at: Universität des Saarlandes, Technische Chemie, Campus C4.2, D-66123 >Saarbrücken. Tel.: +49 681 30264119; fax: +49 681 3022343.
E-mail address: k.stoewe@mx.uni-saarland.de (K. Stöwe).

0920-5861/$ – see front matter © 2010 Elsevier B.V. All rights reserved.
doi:10.1016/j.cattod.2010.07.010

as solubility in water or enhanced quantum yields due to core-shell interactions. Furthermore, the method should allow to be carried out in parallel, easily be automated and give sufficient yields.

There are several well-described methods for the preparation of metal chalcogenide nano-materials in the literature [17–31]. We investigated in preliminary studies hydrothermal and solvothermal synthesis methods, as well as pyrolysis of metal precursors in the presence of coordinating solvents (TOP/TOPO synthesis strategy), which are not reported here. A solvothermal inverse microemulsion approach seemed to be the most promising way to realise all the requirements described above. A microemulsion is a thermodynamically stable dispersion consisting of oil, water and one or more (co)-surfactants. In the case of an inverse (w/o) microemulsion (ME) nano-scaled water droplets are formed in the oil phase. These droplets act as nano-reactors and limit the size of the formed particles to the nano-regime. The surfactant used may also act as stabiliser for the nanoparticles. The solvothermal approach was considered for the specific reason that nanocrystalline materials should be obtained. This is only achievable, if the product formation is controlled. A slow release of sulphide anions offers the possibility of a controlled product formation. Ideally, the sulphide source precursor would only be soluble in the oil phase and slowly release sulphide ions upon decomposition. This decomposition can be achieved by heating. The metal precursor should be easily water soluble and thus remain in the water droplets. Upon diffusion of the sulphide into the water droplets and hydrolysis, the metal sulphide is slowly formed by homogeneous precipitation reactions revealing several advantages compared to heterogeneous precipitation as for instance good crystallinity. TMTMS (tetramethyl thiuram monosulphide) was identified as a suitable precursor. In the following sections, the results of these experiments are presented. Based on the results, the synthesis strategy was improved and a first step in the direction of high-throughput experimentation was undertaken with the development of a 9-fold parallel synthesis reactor.

2. Experimental

All chemicals were purchased from Sigma–Aldrich, Alfa Aesar or ABCR with high purities and were used as supplied. The non-ionic surfactants NP5, NP10 (nonylphenol polyethylene glycol ether) and Triton X-45 (4-(1,1,3,3-tetramethylbutyl)phenyl–polyethylene glycol) were bought from Fluka and were used without further purification.

The microemulsions were prepared by slowly adding the water (16 wt.%) to a mixture of the oil cyclohexane (56 wt.%) and the surfactant mixture of NP5/NP10 or X-45/NP10 (28 wt.%). After a short time of stirring a transparent solution was formed.

For the precipitation of CdS with thioacetamide as precipitation precursor reagent 1.542 g $Cd(ClO_4)_2{\cdot}4H_2O$ (5 mmol) were dissolved in 100 mL of 8% aqueous ammonia solution and subsequently 0.376 g C_2H_5NS (5 mmol) in deionized water were added. Both solutions were stirred at ambient temperature for 2 h. The formed yellow precipitate was separated from the reaction suspension via ultra filtration. The membrane filtration was carried out with 10 kDa UF membrane disc filters from PALL Life Sciences in combination with a vacuum filtration unit from Sartorius Corp. The product was washed several times with deionized water.

2.1. Hydrothermal method

0.392 g $Cd(ClO_4)_2{\cdot}4H_2O$ (1.25 mmol) were dissolved in 25 mL of 8% aqueous ammonia solution and transferred into a Teflon inlet of a 50 mL steel autoclave. 0.262 g TMTMS (1.25 mmol) were added in its solid form to the metal precursor containing solution. The sealed autoclave was placed in a custom made oven and heated to T = 199–207 °C during t = 3 h. The oven was switched-off after 66 h and the autoclave left to cool down naturally to RT. The formed yellow precipitate was separated from the reaction suspension via an ultra filtration. The membrane filtration was carried out with 10 kDa UF membrane disc filters from PALL Life Sciences in combination with a vacuum filtration unit from Sartorius. The product was washed several times with deionized water.

2.2. Solvothermal microemulsion method

The metal precursor, such as $Cd(NO_3)_2{\cdot}4H_2O$, was dissolved in a NP5/NP10 containing microemulsion by stirring with a magnetic bar. A typical concentration would be 0.1 M in regard to the water content of the microemulsion.

The reaction solution was then transferred to a PARR steel autoclave (vol. 300 mL) and a stoichiometric amount of TMTMS was added. The autoclave was sealed and heated to T = 199–213 °C for 4 days. Temperature control was achieved by means of a thermocouple which was positioned at the outer sidewall of the steel autoclave. The pressure reached 9 bar for the described system during the synthesis. The yellow solid product formed was separated from the microemulsion either by centrifugation or membrane filtration. Typically, an ethanol/water (70:30 vol%) washing mixture was added to the product suspension and the suspension was centrifuged for t = 6 min at U = 4500 rpm. The supernatant solution was decanted and the washing process was repeated for three times. The obtained powder was dried in vacuum at T = 50 °C.

As solvothermal microemulsion test setup a standard silica glass ampoule was used and filled with ME. The volume of the ME in the ampoule was chosen so that an autogenic pressure of 9 bar would not be exceeded. The tube was dipped into liquid nitrogen until the ME was completely frozen and then evacuated at a Schlenk vacuum line. Then the tube was sealed and covered with steel wire mesh for safety reasons. The tube was placed in upright position in an oven and gradually heated. The ongoing phase changes were observed.

2.3. Microemulsion method with Lawessons's reagent (LR)

The metal precursor, such as $Cd(NO_3)_2{\cdot}4H_2O$, was dissolved in an argon purged microemulsion in a Schlenk flask by stirring with a magnetic bar. A typical concentration would be 0.1 M in regard to the water content of the microemulsion. Then an equal molar amount of Lawesson's reagent (LR, 2,4-bis-(4-methoxyphenyl)-1,3-dithia-2,4-diphosphetane 2,4-disulphide) was added. The reaction mixture was stirred with a magnetic bar at T = 41–51 °C for 4 days under argon. The precipitated solid product was separated by centrifugation as described previously.

2.4. Microemulsion method with H_2S gas

The metal precursors were dissolved in the microemulsion and transferred to the autoclave. The autoclave, as reaction chamber, consists of the following parts: a 300 mL steel vessel with a teflon inlet and a head with three notches; one notch was connected to the gases H_2S and Ar, the second is connected to ammonia gas and the third to a manometer and sealable gas outlet. The gas outlet was connected to two washing bottles. Frits for better gas dispersion may be fitted to the inside of the autoclave at the gas inlet ports. For all connections and tubings Swagelok components were used.

In a normal reaction sequence the autoclave was flushed with argon, and then, depending on the desired pH in the microemulsion, NH_3 may be bubbled through the vessel. Subsequently H_2S was led into the microemulsion. Flow rates between 0.8 mL/min and fast pressurisation of the chamber up to 10 bar H_2S were possible, depending on the tubing chosen and primary pressure. The precipitated product was separated by centrifugation or membrane filtration as described previously.

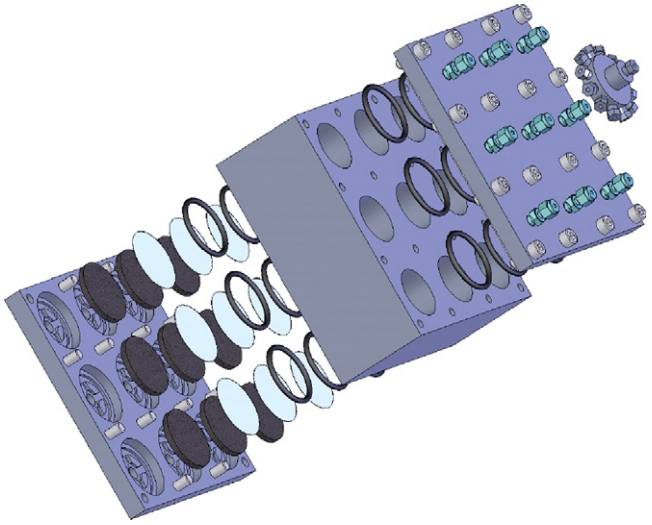

Fig. 1. Explosion view of reactor setup (as used for pressureless synthesis and filtration).

A steel reactor block (stainless steel, WKN 1.4571) with nine individual 100 mL reactors was CNC milled in the machine shop. An exploded view of the setup is shown in Fig. 1. The desired functionality of NP synthesis and filtration of the resulting products in one setup was introduced by different lids. The reactor top lid possesses 9 inlets, each centred above one reactor well. The inlets are connected to a central gas distribution valve (1 top inlet, 12 side outlets). This manifold serves as central gas as well as washing solution distributor to each reactor well. Stainless steel tubes of 3 mm diameter from Swagelok were used. A membrane filtration unit was built into the bottom lid for each reactor. O-rings seal the reactor wells and prevent any cross flow between them. The described setup allows different synthesis approaches. A pressurisation with H_2S or a slow introduction of H_2S by applying small flows is possible. Small flows are realised using capillaries as flow restrictors. The desired flow is regulated by adjusting the H_2S pressure on the manifold. Capillaries are placed inside the reactors at gas inlets, which immersed into the reaction mixture. The small gas bubbles, which are formed due to the very small capillary tubing diameter, ensure good gas dispersion in the microemulsion. After a synthesis the reactor capillaries are removed and the H_2S gas supply is exchanged via Quickfit connections with a washing solution supply for membrane filtration. Typically, 1–2 L of an ethanol/water mixture was sufficient to remove all salt contaminations from the precipitate. A filtration pressure of $p = 5$ bar was applied. The spread of the liquid amount running through each reactor lies below 10%. After washing the membranes with the product they are removed from the reactor and dried in a vacuum oven at $T = 50\,^{\circ}C$.

2.5. Characterisation

The powder X-ray diffraction patterns (PXRD) were collected using either a Huber Guinier camera G670 with a crystal monochromator using $CuK_{\alpha 1}$ radiation ($\lambda = 1.54056$ Å) and an image plate detection system or a PANalytical X'Pert XRD diffractometer in θ/θ – geometry and PIXcel detector with an 15-fold auto sampler using Ni-filtered Cu radiation. The diffraction patterns were evaluated using either FORMFIT [35] or X'Pert HighScore Plus software [36]. The structures were allocated using the ICSD database. The crystal structure parameters and particle size analysis values were refined with the program TOPAS using the fundamental parameter approach [37]. Particle sizes are specified as average column heights, which correspond to particle size directly only in the case of spherical particles. Otherwise correction factors have to be applied depending on particle shape.

The TEM images were taken on a Philips CM200 FEG instrument. The samples were prepared by dispersion of the powders in ethanol supported by ultrasonic radiation. A drop of the dispersion was applied to a 3.05 mm carbon film on an Au grid from Plano Corp.

X-ray fluorescence energy dispersive analysis (XRF-EDX) was performed with the micro X-ray fluorescence spectrometer EAGLE μProbe II from Roenalytic Corp. The instrument is equipped with a Rh X-ray tube. For qualitative analysis the energy signals obtained were compared with theoretical energy line positions. Quantitative analysis was performed using a standardless fundamental parameter model. For the analysis of zinc and copper sulphides standard samples prepared from commercial available powders had to be used to achieve reasonable results. For ternary sulphides this procedure was not practicable. In these cases the sulphur content is underestimated by the analysis method making the metal to sulphur ratio not reasonable. But to indicate a formation of solid solutions these samples are also specified in Table 3 and are especially denoted. Elements with lower atomic number Z <13 can not be quantified, i.e. especially the oxygen content of the samples remains undetermined.

3. Results and discussion

One objective of our research was to find suitable precursors for the controlled release of sulphide species in the water micelles of a microemulsion. Upon hydrolysis at the oil/water interface to $H_2S/HS^-/S^{2-}$ the sulphide species should lead to the formation of metal sulphide nuclei in the water droplets of the ME. The water droplets should restrict the resulting particle sizes of the metal sulphides, which formed to the nano-scale regime. Initially, TMTMS was identified as promising precursor due to its solubility properties. The slow reaction kinetics of TMTMS at room temperature resulted in the formation of N,N′-dimethyl(thio)carbamate salts and made the application of solvothermal reaction conditions necessary to complete the hydrolysis. Nanoparticles were obtained for some metals, but no control of particle size was achieved by varying the ME properties. A solvothermal microemeulsion test setup was used to visually observe the microemulsion at the test conditions and proved that the ME was not stable at solvothermal reaction conditions. Consequently, a precursor was selected which did not require such harsh reaction conditions as TMTMS. Such a precursor was found with Lawesson's reagent. The controlled synthesis of metal sulphide nanoparticles with this precursor was successful. Unfortunately, the formation of metal–organic complexes prevented an application to a broader range of metals. Finally, H_2S gas was tested as precursor.

For the following discussions cadmium and zinc sulphides were selected as examples. Additional data are summarized in the tables. Special attention will be given to degree of crystallinity, phase formation and mechanism.

3.1. Syntheses with TMTMS

Initially, the suitability of TMTMS as precursor for hydrogen sulphide release was tested in a NP5/NP10-ME at ambient conditions. TMTMS is not soluble in water, but is readily dissolved in the oil phase of the ME. Reaction times of 1 day at 50 °C under reflux resulted in a bright yellow product revealing a powder diffraction pattern of a new phase of unknown crystal structure with no relations to the zinc dimethyldithiocarbamate diffraction pattern [38]. Partial hydrolysis may also result in mixed dimethyldithiocarbamate dimethylthiocarbamate salts. All in all, the release of the sulphide species by TMTMS was clearly too slow to result directly in sulphide formation. Solvothermal reaction conditions should

Table 1
Results for the solvothermal synthesis of CdS and mixed (Cd,Zn,Mn)S with TMTMS as precursor.

Sample	T [°C]	t [h]	$c_{reactant}$ [mol/L]	Phase composition (XRD) cub/hex [%]	Particle size (XRD) cub/hex [nm]	Yield [%]
1a	200	66	0.05	15/85	86/48	55
2a	200	96	0.31	66/34	47/47	88
3a	150	15	0.3	–	20/33	–
4a	150	42	0.31	–	42/23	72
5a	150	50	0.31	–	51/31	74
6a	150	52	0.04	–	38/42	61
7a	150	52	0.025	100/0	23	48
8a	150	62	0.1	–	37/34	74
9a	150	52	0.05	63/37	53/19	55
10a	150	52	0.1	60/40	48/14	67
11a[a]	150	52	0.05	80/20	30/22	64
12a[a]	150	52	0.1	77/23	35/38	94
13b	150	62	0.04/0.005/0.005	–	15/8	84
14a	200	52	0.1	–	126/66	56

Sample "a": CdS; "b": $(Cd_{0.8}Zn_{0.1}Mn_{0.1})S$.
[a] Smaller molar water to surfactant ratio R.

considerably enhance the kinetics of the sulphide release by TMTMS and increase the hydrolysis rate to S^{2-} at the oil/water interface in the ME.

Therefore TMTMS as precursor for hydrogen sulphide release was tested under hydrothermal conditions (see Table 1, sample 1a). PXRD measurements revealed that the reaction yielded mainly hexagonal CdS nanoparticles (NP) and a smaller amount of larger cubic CdS NP. The formation of CdS with good yields proves the release of the sulphide species upon heating. The results are comparable with previously hydrothermally synthesised CdS NP using different reagents [32].

Subsequently, the influence of the reaction temperature, reaction time and reactant concentration was investigated. Additionally, the composition of the ME was modified with regard to the water content. Reactant concentrations are an important parameter in ME nanoparticles synthesis. The concentration may take a strong influence on the resulting particle sizes. The degree of influence depends on the dominant growth mechanism of the particles in the microemulsion. If, for instance, the particle growth follows strictly the LaMer diagram, lower reactant concentrations yield smaller particles sizes [40–42]. Regarding the ME, the molar ratio of water to surfactant R may modify also the NP size. Both parameters were investigated (see Table 1).

It should be considered, that sphalerite – wurzite polymorphism commonly occurs and that this polymorphism is one-dimensional, i.e. polytypism, which may be also regarded as stacking order variations in the particles alternatively to different particles with an either cubic or hexagonal structure. Furthermore, also more complicated stacking sequences are possible for a sample [43]. This might be illustrated for two samples from very different synthesis routes, as shown in Fig. 2. Fig. 2 shows the diffraction pattern and Rietveld refinement results of CdS prepared by the solvothermal TMTMS (top) and the thiourea route (bottom). In the first case the crystallite size is rather large ($L > 50$ nm) and clearly the two polytypic forms with different symmetry can be identified. In the second case with thiourea as precipitant the particle size is very small ($L < 4$ nm) and striking feature of the diffraction pattern is the almost complete absence of the (0 0 2) reflection of the cubic phase at $2\theta \approx 30^\circ$ and the (0 1 2) reflection of the hexagonal phase at $2\theta \approx 36^\circ$ resulting in deviations in intensity in the Rietveld refinements using a model with separate cubic and hexagonal phases. Alternatively, the diffraction pattern can be interpreted by a model with completely randomized stacking sequence. For this purpose, a unit cell with the smallest common multiple of both sequences, i.e. six most dense packed atom layers, has been assumed and an isomorphic crystallographic subgroup of the wurzite type, i.e. space group $P6_3mc$, taken for refinement. The atomic coordinates have been transformed into this new cell ($a = 0.419(1)$ nm, $c = 2.080(3)$ nm and $L = 2.9(1)$ nm) and fixed to the special values of the sphalerite structure-type. The average crystallite dimensions are in this case not much larger than the unit cell and the clear separation between hexagonal and cubic stacking sequences are smearing in the nanoparticles. Simultaneously we have reached the limitations of the diffraction method. The same alternative interpretation exists for the samples from the HT reactor setup (see below).

Regarding the particles sizes obtained, especially at different concentrations and water volumes, it becomes evident that the size changes are rather small. Furthermore, the overall particle sizes are rather large. A control of the particle size, as usually observed for microemulsion synthesis methods at RT, seems in this case not possible. Difficulties in controlling the particle sizes for a solvothermal ME system were also reported previously [39].

In order to gain a better understanding of the solvothermal ME system, a simple test setup was developed for the observation of the ME under reaction conditions. At the reaction temperature ($T = 150$ °C), two phases were present; a slightly clouded upper phase and a lower milky opaque phase. When the temperature was increased to $T = 200$ °C, a total phase separation was observed. A small lower clear phase was formed and an upper slightly clouded phase. The phase separation behaviour is described in the literature for non-ionic surfactant microemulsion systems at elevated temperatures [44]. Probably a nearly pure water phase is formed as lower phase, whereas the upper phase consists of a surfactant rich oil phase. The exact composition or structure was not investigated for the upper phase.

This result indicates that not a solvothermal ME synthesis is taking place but rather a process similar to a hydrothermal synthesis. There seems to be some limitation to the growth of NP compared to the purely hydrothermal synthesis by the surfactant molecules present, but no true control over the particle size seems to be possible. Apart from this, the synthesis method was not applicable to the formation of a broader range of metal sulphides. The products obtained for other metals at reaction conditions similar to the CdS syntheses were mainly metal–TMTMS complexes or even absence of product formation at all was observed. Consequently, a system, working at RT or just below the clouding point of the ME seemed to be a more promising approach.

3.2. Syntheses with Lawesson's reagent (LR)

The new precursor LR was tested, which slowly releases sulphide anions when it is dissolved in water. In first test reactions CuS, CdS and In_2S_3 precipitated from an aqueous solution containing the metal nitrates as reactants. PXRD patterns showed

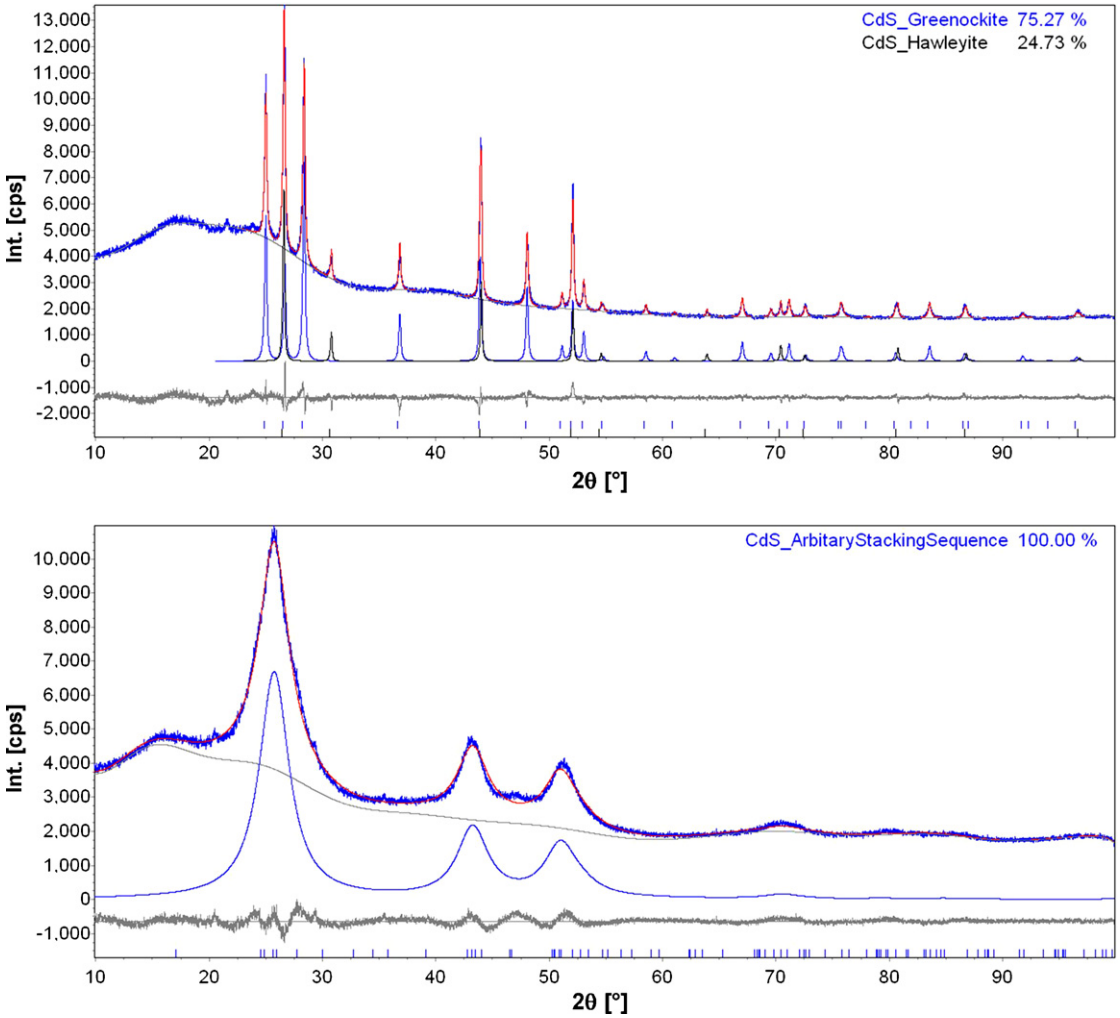

Fig. 2. PXRD patterns and TOPAS-Rietveld refinement results of CdS prepared by the solvothermal TMTMS route (sample 14a, top) and the thiourea route (bottom). Background intensity modulation in the 2θ-range between 18° and 28° are due to the Tesa tape used for sample preparation.

that the obtained products were amorphous or only partially crystalline. A possibility to enhance crystallinity is an increase in reaction temperature. Further test reactions were carried out in microemulsions at 41 °C or 51 °C (just above the clouding point) (see Table 2).

CdS was not formed at a reaction temperature of T = 41 °C (sample 14a). The separated solid consisted of an undefined coordination complex of LR with Cd ions. Amorphous CdS was obtained for a reaction temperature of T = 46 °C (sample 13a). At T = 51 °C small NP of hexagonal symmetry were obtained (sample 15a, 94%, L = 5 nm). Also a small amount of larger cubic CdS NP was formed (6%, L = 19 nm).

For ZnS even at the lowest temperature investigated (sample 16c, T = 41 °C) no complexes were formed. Only nuclei formation of the cubic phase occurs (L = 3 nm). At T = 51 °C the symmetry of the predominantly formed phase is hexagonal (L = 7 nm) and the average size of the cubic crystals remains equal to that of sample 16c, the crystal sizes of both phases being rather small.

Investigations referring to nanocrystal nucleation and growth in microemulsions are not reported in the literature. But detailed insights to the kinetics of semiconductor nanocrystal formation for liquid phase colloidal synthesis methods from precursor molecules in high temperature and coordinating solvents like tri-*n*-octylphosphine (TOP) or tri-*n*-octylphosphine oxide (TOPO) are found due to the possibility of minimizing polydispersity by careful control of synthesis parameters as temperature and additive concentration [45,46]. For instance Rempel et al. [45]. developed a model for nanoparticle growth combining an activation mechanism for precursor conversion to monomers, discrete rate equations for formation of small-sized clusters, and a continuous Fokker–Planck

Table 2
Reaction conditions and results for LR ME synthesis of CdS and ZnS.

Sample	T [°C]	t [h]	c_{metal}/c_{LR} [mol/L]	Phase composition (XRD) cub/hex [%]	Particle size (XRD) [nm]	Yield [%]
13a	43–46	64	0.1/0.1	amorphous	–	–
14a	41	96	0.1/0.12	no reaction	–	–
15a	51	96	0.1/0.12	6c/94h	19/5	>99
16c	41	96	0.1/0.12	100c	3	48[a]
17c	51	96	0.1/0.12	23c/77h	3/7	>99

Sample "a": CdS; "c": ZnS.
[a] Lowered yield due to experimental error.

equation for growth of large-sized particles. In this paper the emphasis is on the particle size distribution, their focusing and defocusing, but no polymorphic phase transformations are discussed. Cozzoli et al. [46] discuss the shape and phase control of colloidal ZnSe nanocrystals under similar synthesis conditions in terms of classical nucleation theory (CNT), which might be not suitable to describe nucleation at the nano-scale [45]. On the other hand coarsening of nanocrystalline ZnS under hydrothermal conditions together with size-dependent phase transformation kinetics have been described by Huang and Banfield [47]. Whereas bulk wurzite ZnS is metastable relative to sphalerite below temperatures of 1020 °C at low pressure, they observed under hydrothermal conditions that sphalerite transforms to wurzite at 225 °C and conclude that nanocrystalline wurzite is stable at low temperatures. In bulk materials the phase transformations are generally complex due to a high defect concentration, which is usually absent in nanocrystals. Phase transformations of sphalerite to wurzite in bulk materials have been explained in terms of a periodic slip mechanism involving expansion of stacking faults around an axial screw dislocation. In nanocrystalline materials oriented attachment (OA) introduces twin and stacking fault formation during the crystal growth process. XRD analyses showed that there is no detectable wurzite in the croasened sample prior to the onset of Ostwald ripening. According to HRTEM images wurzite nucleated on the surface of sphalerite nanoparticles after a growth phase. The authors state that traditional transformation kinetic models are inconsistent with the transformation kinetics observed in nanocrystalline ZnS as they do not predict a cessation of transformation at longer reaction times, when the nanocrystals growth reached a critical size of 22 nm. At longer reaction times phase transformation activation energy in nanoparticles is much smaller than that in bulk ZnS due to the size limitation of the particles. In their models nucleation occurs at the surface and growth involves collective movement of atoms at the wurzite–sphalerite interface. Their data are consistent with a phase stability of wurzite at small particle sizes (3–7 nm). This is just the particle size range we observed in our experiments. At a temperature of 41 °C only meta-stable cubic phase nanocrystals of very small size (L = 3 nm) are formed. Ten degrees higher in reaction temperature at the same reaction time the transformation rate is higher, so that Ostwald ripening occurred and most of the meta-stable cubic phase had transformed into a hexagonal wurzite phase with somewhat higher particle size. As the average particle size of the cubic phase has been very small no significant change in this parameter is observed on ripening. As already observed by Huang et al. at low temperatures the wurzite form of ZnS is the stable phase for nanocrystals.

The next step was the synthesis of a broader range of metal sulphides and mixed metal sulphides. The reaction conditions were equal to the synthesis of samples 14a and 17c. In many cases the compounds formed were LR–metal complexes or no product formation was observed at all. Although LR was suitable to obtain small well-crystalline NP for some metals, it is not suited for a high-throughput approach with a broad range of metals. The possible range of accessible metal sulphides may be enlarged by further optimisation of the reaction conditions and change of the reaction media, but this approach was not followed up further.

3.3. H_2S syntheses

Regarding the results obtained so far, it becomes obvious, that the release of the sulphide species and the formation of the metal sulphide are the crucial steps. The system dependent formation of precursor–metal complexes and the chemistry of the sulphides (solubility product, pH-dependency) proved to be the main challenges. The slow release of the sulphide species in a microemulsion proved to be effective for the synthesis of crystalline NP. An ideal precursor would not form complexes with the metals or require elevated temperatures for the release of the sulphide species. The necessary reaction conditions should not lead to larger changes of the microemulsion properties as for instance micelle size distribution. For these reasons we decided to use H_2S as direct sulphide source. With H_2S quite a broad range of metal sulphides can be directly precipitated from aqueous solutions. Some metal sulphides require basic reaction conditions. The introduction of the base into the solution in order to adjust the pH, the most crucial parameter during precipitation, was solved by using gaseous NH_3 where necessary.

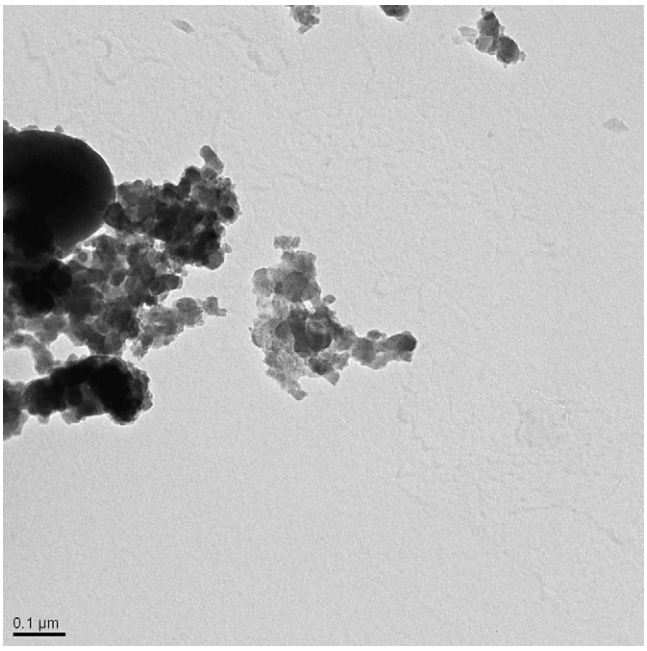

Fig. 3. TEM image of $PdS_{1.7}$ (scale bar corresponds to 100 nm, sample 47).

Two approaches were tested. One approach was the pressurisation of the metal precursor containing microemulsion with H_2S gas. The other approach was the slow dispersion of H_2S gas into the metal precursor containing microemulsion. The results of the two routes are summarized in Table 3. The pressure route yielded mainly amorphous products or small NP which were only partially crystalline. The slow introduction of the sulphide source gave generally better results. Smaller particle sizes and improved crystallinity were observed.

Various amorphous noble metal sulphides could be synthesised by the pressurisation route (samples 47–50, 52–57). Among these the palladium sulphides were investigated more thoroughly. The applied H_2S pressure had a direct influence on the morphology of the precipitated product for palladium sulphides (samples 47 and 49): at a pressure of 10 bar a partially crystalline compound was obtained (Fig. 3). Energy dispersive X-ray spectrometric (EDX) analysis resulted in a composition of palladium disulphide substoichiometric in sulphur. At a pressure of 0.5 bar H_2S an X-ray-amorphous phase was obtained. TEM investigations clearly showed small agglomerated NP with sizes around L = 2–6 nm (see Fig. 4). From EDX analyses again a composition of palladium disulphide substoichiometric in sulphur ($PdS_{1.8}$) followed. Pressureless introduction of H_2S gas into the ME at high flow rates gave amorphous $PdS_{1.5}$ (sample 45). Lower flow rates of 0.8 mL/min gave amorphous palladium sulphide of the composition $PdS_{1.6}$ (samples 44 and 46). When a freshly precipitated amorphous palladium sulphide was stirred for a period of 18 h at T = 47–48 °C, the PXRD patterns remained unchanged. Therefore ageing effects can be excluded. As

Table 3
Reaction conditions and results for H_2S ME synthesis of various metal sulphides and mixed metal sulphides.

Sample	Elements	Flow H_2S mL/min	p H_2S/(p NH_3) [bar]	t [h]	c_{metal1} ($/c_{metal2}$) [mol/l]	Phase composition (XRD) [%]	Phase composition (XRF) [at %]	Particle size (XRD) [nm]	Yield [%]
18	Cd	0.8		12	0.1	33c/67h	–	11/5	94
19	Cd	[a]		0.5	0.1	57c/43h	$Cd_{50}S_{50}$	12/9	47
20	Cd	0.8		3	0.1	31c/69h	$Cd_{50}S_{50}$	10/5	65
21	Cd		0.2	60	0.1	20c/h80	$Cd_{48}S_{52}$	17/4	52
22	Cd		5	15	0.1	42c/58h	$Cd_{47}S_{53}$	7/9	93
23	Zn	0.8		3	0.1	cub ZnS	$Zn_{49}S_{51}$	6	83
24	Zn		5	72	0.1	83c/17h	$Zn_{50}S_{50}$	19/10	
25	Cu	0.8		3	0.1	hex CuS	$Cu_{50}S_{50}$	10	40
26	Cu/Zn	0.8		17	0.09/0.01	hex CuS	–	7	36
27	Cu/Zn	0.8		21	0.09/0.01	hex CuS	–	7	92
28	Cu/Zn	0.8		12	0.09/0.01	hex CuS	$Cu_{57}Zn_4S_{39}$[b]	9	50
29	Cu/Fe		2	2	0.09/0.01	hex CuS	$Cu_{61}Fe_2S_{37}$[b]	6	–
30	Cu		1	24	0.1	CuS	$Cu_{58}S_{42}$	amorph.	70
31	Cu		1	72	0.1	CuS	$Cu_{49}S_{50}$	amorph.	>99
32	Cu/Zn		5	24	0.09/0.01	hex CuS	$Cu_{61}Zn_6S_{33}$[b]	14	78
33	Cu/Ni		6	0.5	0.09/0.01	hex CuS	$Cu_{55}Ni_4S_{41}$[b]	16	92
34	Fe/Co	0.8		12	0.09/0.01		$Fe_{27}Co_1S_{72}$[b]	amorph.	78
35	Fe/Co	0.8		12	0.09/0.01		$Fe_{24}Co_2S_{73}$[b]	amorph.	136[c]
36	Fe/Mn	0.8		12	0.09/0.01		$Fe_{88}Mn_{10}O_xS_2$	amorph.	56
37	Fe/Mn	0.8		12	0.095/0.005		$Fe_{50}Mn_3S_{47}$[b]	amorph.	79
38	Fe		10	1	0.09/0.01		$Fe_{45}S_{55}$	amorph.	91
39	Fe		10	0.2	0.1		$Fe_{50}S_{50}$	amorph.	>99
40	Fe/Co		10	24	0.09/0.01		$Fe_{74}Co_9S_{17}O_x$[b]	amorph.	115[c]
41	Fe/Co		10	1	0.09/0.01		$Fe_{66}Co_6S_{27}$[b]	amorph.	137[c]
42	Fe/ Mn		10/(7)	1.5	0.09/0.01		$Fe_{47}Mn_5S_{48}$[b]	amorph.	91
43	Fe/Mn		10/(6)	1	0.095/0.05		$Fe_{54}Mn_3S_{44}$[b]	amorph.	76
44	Pd	0.8		2	0.1		$Pd_{39}S_{61}$	amorph.	99
45	Pd	20		3	0.1		$Pd_{39}S_{61}$	amorph.	64
46	Pd	0.8		12	0.1		$Pd_{38}S_{62}$	amorph.	113[c]
47	Pd		5–10	12	0.1		$Pd_{37}S_{63}$	amorph.	70
48	Pd		10	12	0.05		$Pd_{30}S_{69}$	amorph.	60
49	Pd		0.5–1	12	0.1		$Pd_{36}S_{64}$	amorph.	30
50	Pd		0.5	12	0.1		$Pd_{36}S_{64}$	amorph.	95
51	Ni	0.8		3	0.1	unknown	$Ni_{29}S_{71}$	cryst.	42
52	Pt		10	12	0.1		$Pt_{35}S_{65}$	amorph.	>99
53	Rh		10	12	0.1		$Rh_{40}S_{60}$	amorph.	99
54	Ir		10	90	0.1		$Ir_{21}S_{79}$	amorph.	
55	Ru		10	12	0.1		$Ru_{39}S_{61}$	amorph.	94
56	Au		10	12	0.28		$Au_{38}S_{61}$	amorph.	74
57	Re		10	12	0.1		$Re_{34}S_{66}$	amorph.	99
58	Mo		10	12	0.1		MoS_x	amorph.	
59	La		10/(6)	2	0.09/0.01		$La_{14}Y_2Pr_2S_{81}$	amorph.	75

[a] Saturated H_2S ME given to metal containing ME.
[b] Standardless quantification – underestimation in S content.
[c] Too high yields may be due to polysulfide formation and unknown oxygen content.

both palladium sulphides with S: Pd ratio ≥1 are Pd(II) sulphides, the products formed (PdS_x, $x > 1$) are most probably mixtures of the two phases known in the literature, PdS and PdS_2. Additional investigations by X-ray absorption spectroscopy (XAS) in progress will clarify the oxidation states of the contributing elements.

Various non-precious metals sulphides and mixed metal sulphides were also synthesised by both routes. Only the cadmium and zinc sulphides will be here discussed again in more detail (see Table 3).

For zinc sulphide at H_2S gas flow of 0.8 mL/min only a crystalline cubic phase with a particle size of $L = 6$ nm was formed (sample 23). At $p = 5$ bar reaction pressure the cubic phase was predominantly formed (83%) with a NP size of $L = 19$ nm, but also a smaller amount (17%) of hexagonal phase with a particle size of $L = 10$ nm. The particle sizes at elongated reaction times (72 h compared to 3 h) were much larger for the pressurisation route.

The structural chemistry of these compounds is very similar. The lattice energy differences, as previously mentioned, for the hexagonal and cubic phases of these sulphides are low and depend on particle size. As the energies differences are so small, polytypism is commonly observed. Particles were formed with stacking order variations. For ZnS at low pressures we again (see Section 3.2) observe for short reaction times almost complete formation of the sphalerite phase with average particle sizes of $L = 6$ nm. At 5 bar pressure two parameters have been varied and at the longer reaction times Ostwald ripening had already occurred and some of the cubic phase transformed into the hexagonal phase together with a particle size increase, an observation, which has already been found for the ZnS nanocrystals synthesised by precipitation with the LR.

In contrast to ZnS, for CdS we find even at short reaction times and pressureless H_2S addition a mixture of both phases of approximate ratio c:h = 1:2 (sample 20, 3 h reaction time, phase ratio 31c/69h and crystallite size $L = 10/5$ nm). On rather short time scales this composition is stable and does not change in phase ratio and particle size (sample 18, 12 h reaction time, phase ratio 33c/67h and crystallite size $L = 11/5$ nm). Regarding $p = 0.2$ bar in the pressurisation route compared to 5 bar almost pressureless, much longer reaction times yielded mainly a CdS phase crystallizing hexagonally with an increased crystallite size of the cubic phase (sample 21, 60 h reaction time, phase ratio 20c/80h and crystallite size $L = 17/4$ nm). During Ostwald ripening the smallest cubic nanocrystals dissolved in favour of the formation of new hexagonal ones at the nanocrystal surface of other cubic ones forming new nanocrystal domains, as proposed by Huang and Banfield (see above). A particle growth of

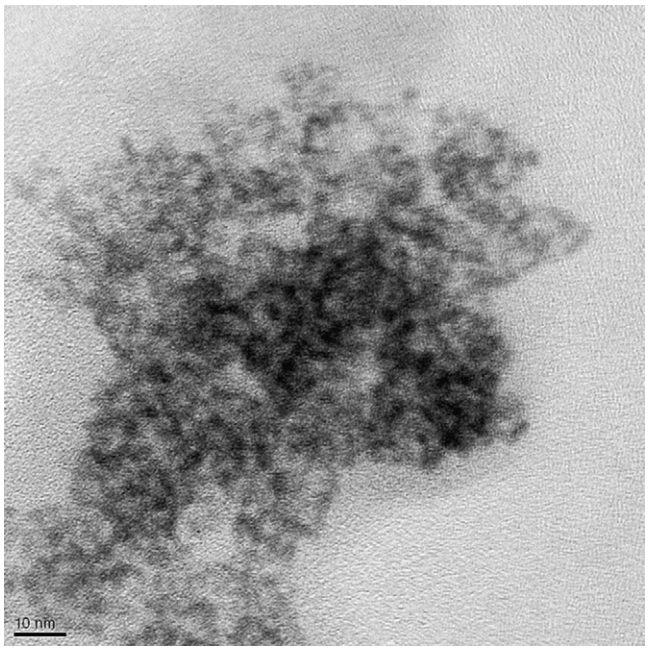

Fig. 4. TEM image of $PdS_{1.8}$ (scale bar corresponds to 10 nm, sample 49).

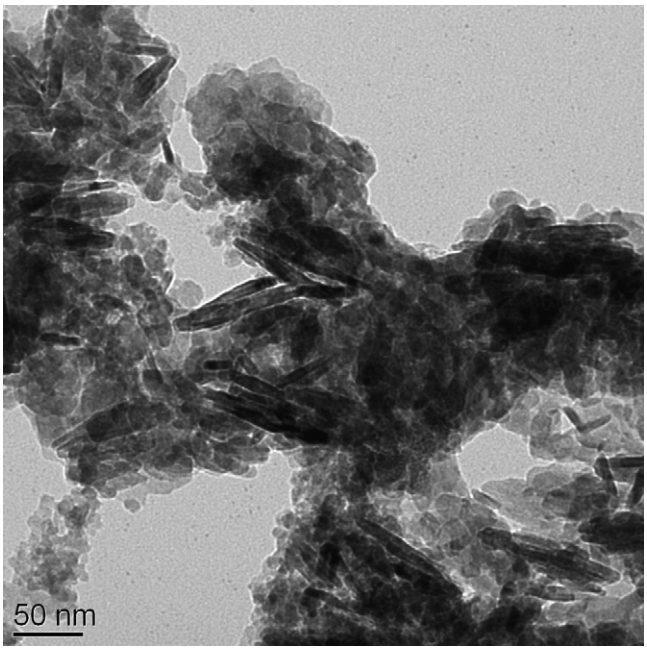

Fig. 5. TEM image of needle shaped and spherical agglomerated nanoparticles of $Cu_{90}Zn_{10}S$ (sample 32).

the wurzite type in the meantime is not observed (L = 5 vs 4 nm). The remaining cubic crystals have a larger average size (sample 21, L = 17 nm). Compared to the literature data mentioned above [45–47] the pressurized addition of the sulphide species introduces another parameter, the pressure p. By slow sulphide release, either by an equilibrium reaction starting with the precursor [38,39] or by the dissolution of an existing phase, [47] also an always low concentration of the precipitant is generated (as in the pressureless route), but in the pressurized case a much higher supersaturation is achieved. At a H_2S reaction pressure of 5 bar the crystallite size of cubic phase is again smaller and its phase quantity higher compared to the low pressure approach (sample 22, 15 h reaction time, phase ratio 42c/58h and crystallite size L = 7/9 nm). Supersaturation favours nuclei formation, so that the average particles sizes are smaller. If the particle size reduction to the nano-scale inverts the stability sequence of the bulk material, making the hexagonal phase the stable one and the cubic the meta-stable one, we have to conclude that phase formation in microemulsions occurs via intermediate formation of the meta-stable form, consistent with the Ostwald step rule, and that at higher supersaturation the amount of the meta-stable phase is increased.

In the case of mixed copper sulphides of the general composition $Cu_{90}M_{10}S$ (M = Zn, Ni) crystalline NP were yielded for both synthesis routes (see Table 3 and Fig. 5).

3.4. High-throughput experimentation

The applied H_2S route allows a simple parallelisation of the synthesis process. The use of the 9-fold reactor as a first step towards HTS should not only lead to a faster synthesis of the metal sulphides but also help to faster optimise the syntheses with respect to the effect of precursor, reaction conditions and ME composition on the resulting compounds as variation parameters. Additionally the effect of operating personal as additional error source can be minimized. For the characterisation largely automated systems were used. PXRD analysis was performed with an X'Pert Pro diffractometer system which allows the automated sequential measurement of up to fifteen samples supplied by an autosampler. XRF analysis was performed with an Eagle μProbe II using standard 96-fold well plates. The plates contained up to 25 compounds and the automated measurements were carried out by computer scripts.

The XRD patterns are shown in Fig. 6 for CdS nanoparticles produced in a test run with the 9-fold parallel reactor. The phase composition of each well and the particle sizes obtained by Rietveld refinement are summarized in Table 4. Generally, two modifications of CdS were found in the samples. The high FWHM of the diffraction pattern indicate that the material is nanocrystalline. The peaks for the hexagonal phase (greenocite) and the cubic phase (hawleyite) again partially overlap. In every case the predominant stacking is hexagonal (phase quantity >60%). Particles with sizes ranging from L = 4.0–6.8 nm were formed. For the minor cubic phase particle sizes of L = 8.6–15.6 nm were obtained. For HT8 a reduced reactant metal salt concentration was used (c = 0.076 mol/L instead of 0.1 mol/L). A clearly smaller particle size of L = 3 nm was obtained.

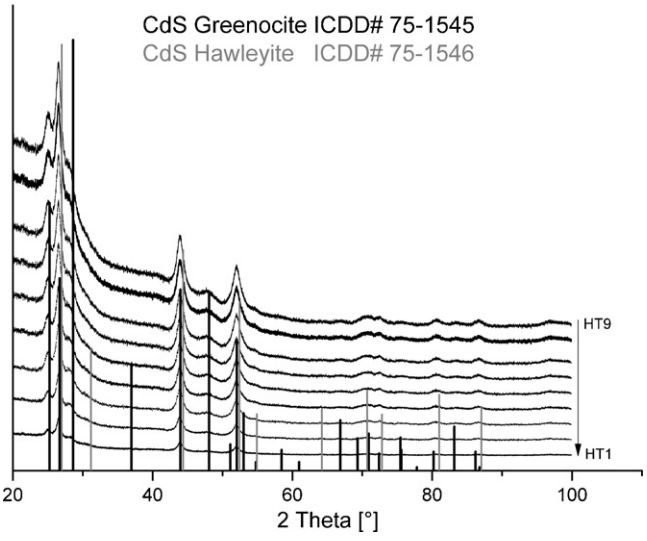

Fig. 6. PXRDs of CdS prepared in the 9-fold reactor; syntheses HT1-7 and HT9 with a precursor concentration of 0.1 mol/L and HT8 with a precursor concentration of 0.076 mol/L.

Table 4
Results of CdS PXRD analysis by Rietveld refinement; samples HT1-9 were prepared in a new HT setup for parallel precipitation reactions as described in the text and Fig. 1; reactant concentration 0.076 mol/L for HT8, 0.1 mol/L for all other reactors.

Reactor	Cubic phase		Hexagonal phase	
	Mean particle size [nm]	Phase quantity [%]	Mean particle size [nm]	Phase quantity [%]
HT1	15.6(2)	37.3	6.5(1)	62.7
HT2	11.9(2)	33.7	6.8(1)	66.3
HT3	8.6(1)	39.7	5.8(1)	60.3
HT4	12.0(5)	21	4.0(1)	79
HT5	7.8(1)	35.9	4.8(1)	64.1
HT6	9.5(2)	29.9	4.7(1)	70.1
HT7	9.0(1)	37.8	5.8(1)	62.2
HT8	11.3(5)	17.1	3.0(1)	82.8
HT9	10.2(2)	32.5	5.4(1)	67.5

Also, with 82.5%, the largest amount of the hexagonal phase in the samples had been observed. An additional experiment with varying cadmium nitrate reactant concentrations was carried out. A general trend of passing a minimum in particle size at concentrations of 0.03–0.05 mol/L was observed (see Fig. 7).

The analyses of the HT reactor results are in good agreement with the results for the pressureless CdS synthesis in the conventional reactor assembly (sample 20). The particle sizes obtained are in the same range of L = 4–6.8 nm (hexagonal) and L = 8.6–15.6 nm (cubic form). The size variations in each reactor were expected because random variations including local variations of concentrations cannot be avoided. The MEs were not especially filtered for impurities (such as dust particles present everywhere). Roughness of the reactor walls and different stirring conditions take further unpredictable influence. Small differences in the gas flow due to small diameter variations of the inlet tubing may also take influence on the resulting particle sizes. The reduced particle size at lower metal salt reactant concentration (HT8) is a clear sign for a particle formation predominantly described by the LaMer diagram. This model describes the variation of resulting particle sizes in dependence of the reactant concentrations and ME aqueous droplet sizes. The diagram explains the precipitation in terms of supersaturation, nucleation and growth. Higher reactant concentrations lead to the formation of larger particles. Assuming that the number of nuclei formed at various reactant concentrations remains constant, an increase in reactant concentration leads to an extended growth period of the particles and therefore results in larger particles.

The LaMer model does not take into account the influence of the surfactant. The adsorbed surfactant molecules may either stabilize or destabilize the particles thermodynamically and this stabilisation effect may be different for different crystal faces, thus influencing also the crystal habit. A particle formation completely governed by thermodynamic stabilisation shows no influence of the reactant concentrations or droplet sizes on the obtained particle sizes. Both models are approximations and in general both processes take influence on the particle formation. The minimum passed in Fig. 7 is an example for a process which is influenced by both growth processes.

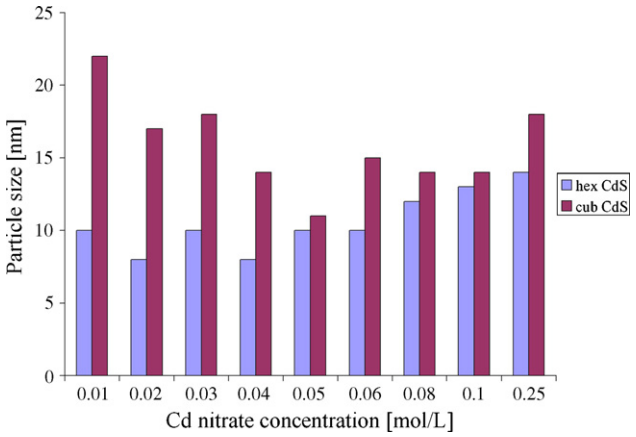

Fig. 7. Resulting CdS particle sizes for varying cadmium nitrate reactant concentrations in the HT reactor setup. The error in particle size determined by Rietveld refinement of the PXRD pattern is less than 1 nm.

With the described HT reactor setup first small compound libraries were synthesised (composition spreads of ternary systems such as Cu–Zn, Cu–Ni, Cu–Fe). In Table 3 these results are given as example for the nominal composition $(Cu_{0.9}Fe_{0.1})S$. PXRD analysis showed that a precipitate was formed with covelite structure and particle sizes of L = 6 nm. EDX analysis additionally confirmed that the iron component is included in the solid material in sample 29.

For the synthesis of mixed metal sulphide composition spreads the solubility limits of the binary metal sulphides in each other have to be recognised. The study of structural stability diagrams and crystal class classifications are necessary. Extensive reviews about the crystal structures and structural classifications are available [48].

4. Conclusion and outlook

Several routes for the synthesis of nano-scaled (mixed) metal sulphides have been presented differing in the degree of appropriateness for the intended objectives, i.e. applicability to a broad range of mixed metal sulphides and potential to be carried out in high-throughput. Several selected precursors (LR, TMTMS) for the synthesis of the nano-scaled metal sulphides form coordination complexes with the metal ions thus limiting the spectrum of compounds to be synthesised. In the case, where hydrolysis of the coordination complexes by solvothermal conditions forces sulphide formation (TMTMS), loss of microemulsion stability results in particle growth. The obtained sulphide particles are still in the nm-range, but are larger than those particle diameters, for which quantum size effects are typically observed. But it should be emphasized that both variants may have a certain relevancy for nanoparticle synthesis in the future. The only way out of this problem might be the usage of non- or weak-coordinating organic sulphides. In the present contribution the choice of H_2S gas as sulphide precursor in combination with a w/o microemulsion led to the successful synthesis of a broad range of amorphous and crystalline materials of the intended compositions and particle sizes.

In a first step towards HTS a 9-fold reactor was constructed, which allows truly parallel synthesis, separation and purification. A further scale-up of this system will allow a fast synthesis of a large number of compounds as required for a combinatorial workflow. All of these materials have unique properties and will be tested in catalytic processes. Methods for stabilisation of the prepared nanoparticles to prevent agglomeration are presently implemented. Additional characterisation of the prepared nano-

scaled sulphides by X-ray absorption spectroscopy (XAS) is also in progress.

Acknowledgement

This project was funded by the German Research foundation DFG. We gratefully acknowledge the help by J. Schmauch, Experimentalphysik, Saarland University (TEM measurements) and R. Richter, Technische Chemie, Saarland University (HT reactor setup construction).

References

[1] M. Breysse, G. Djega-Mariadassou, S. Pessayre, C. Geantet, M. Vrinat, G. Perot, M. Lemaire, Catal. Today 84 (2003) 129–138.
[2] A. de Klerk, Catal. Today 130 (2008) 439–445.
[3] J.W. Gosselink, NATO ASI Series, Series 3: High Technology 60 (1998) 311–355.
[4] J.-F. Paul, S. Cristol, E. Payen, Catal. Today 130 (2008) 139–148.
[5] M. Breysse, C. Geantet, P. Afanasiev, J. Blanchard, M. Vrinat, Catal. Today 130 (2008) 3–13.
[6] H. Knotzinger, NATO ASI Series, Series 3: High Technology 60 (1998) 189–206.
[7] E.J.M. Hensen, J.A.R. van Veen, Catal. Today 88 (2003) 87–109.
[8] Z. Vit, Appl. Catal. A 322 (2007) 142–151.
[9] F. Bataille, J.L. Lemberton, G. Perot, P. Leyrit, T. Cseri, N. Marchal, S. Kasztelan, Appl. Catal. A 220 (2001) 191–205.
[10] J. Heising, M.G. Kanatzidis, J. Am. Chem. Soc. 121 (1999) 11720–11732.
[11] A. F. Gulla, R. J. Allen, World Patent No. WO 2008101955 (2008).
[12] P. W. Glockner, J. D. Richardson, US Patent No. 4078011 (1978).
[13] E. Wilms, G. Michalczyk, US Patent No. 4081404 (1978).
[14] G. C. Chinchen, US Patent No. 4142988 (1979).
[15] J. Zhang, Y. Wang, L. Chang, Appl. Catal. A 126 (1995) 219–227.
[16] B.L. Abrams, J.P. Wilcoxon, Crit. Rev. Solid State Mater. Sci. 30 (2005) 153–182.
[17] T.R. Thurston, J.P. Wilcoxon, Phys. Chem. B 103 (1999) 11–17.
[18] M.A. Malik, N. Revaprasadu, P. O'Brien, Chem. Mater. 13 (2001) 913–920.
[19] P. O'Brien, J.R. Walsh, M. Watson, M. Motevalli, L. Henriksen, J. Chem. Soc., Dalton Trans. (1996) 2491–2496.
[20] S. Biswas, S.K. Hait, S.C. Bhattacharya, S.P. Moulik, J. Dispersion Sci. Technol. 25 (2005) 801–816.
[21] Y. Ding, X. Liu, R. Guo, Colloids Surf. A 296 (2007) 8–18.
[22] P.S. Khiew, N.M. Huang, S. Radiman, M.S. Ahmad, Mater. Lett. 58 (2004) 762–767.
[23] L. Wang, M. Schultz, E. Matijevic, Colloid Polym. Sci. 275 (1997) 593–598.
[24] G.Q. Zhu, P. Liu, Cryst. Res. Technol. 44 (2009) 713–720.
[25] S. Biswas, S. Kar, S. Chaudhuri, Appl. Surf. Sci. 253 (2007) 9259–9266.
[26] M.R. Close, J.L. Petersen, E.L. Kugler, Inorg. Chem. 38 (1999) 1535–1542.
[27] J.S. Wang, A.B. Smetana, J.J. Boeckl, G.J. Brown, C.M. Wai, Langmuir 26 (2009) 1117–1123.
[28] D. Chai, X. Yuan, B. Yang, Y. Qian, Solid State Commun. 148 (2008) 444–447.
[29] Z.Y. Xu, Y.C. Zhang, Mater. Chem. Phys. 122 (2008) 333–336.
[30] R. Rao, H. Chandrasekaran, S. Gubbala, M.K. Sunkara, C. Daraio, S. Jin, A.M. Rao, J. Electron. Mater. 35 (2006) 941–946.
[31] W.F. Maier, K. Stoewe, S. Sieg, Angew. Chem. Int. Ed. 46 (2007) 6016–6067.
[32] D. Farrusseng, Surf. Sci. Rep. 63 (2008) 487–513.
[33] C. Mirodatos, W.F. Maier, M. Aresta, Catal. Today 137 (2008) 1.
[34] M. Seyler, K. Stoewe, W.F. Maier, Appl. Catal. B 76 (2007) 146–157.
[35] R. Haberkorn, ERLRAY Program for the Interpretation of X-ray powder diffraction pattern, Dudweiler (1998).
[36] X'Pert HighScore Plus V2.2c: Complete Full Powder Pattern Analysis Tool, PANalytical B.V., Almelo, The Netherlands, 2007.
[37] TOPAS V2.1: General Profile and Structure Analysis Software for Powder Diffraction Data, Bruker AXS, Karlsruhe Germany, 2003.
[38] H.P. Klug, Acta Crystallogr. 21 (1966) 536–546.
[39] P. Zhang, L. Gao, J. Colloid Interface Sci. 272 (2004) 99–103.
[40] V.K. LaMer, R.H. Dinegarn, J. Am. Chem. Soc. 72 (1950) 4847–4854.
[41] T. Sugimoto, Adv. Colloid Interface Sci. 28 (1987) 65–108.
[42] L. Jeunieau, F. Debuigne, J.B. Nagy, Reactions and Synthesis In Surfactant Systems, Marcel Dekker, Inc., New York, 2001.
[43] A.S. Vorokh, A.A. Rempel, Phys. Solid State 49 (2007) 148–153.
[44] G.R. Deen, C.L.P. Oliveira, J.S. Pedersen, J. Phys. Chem. B 113 (2009) 7138–7146.
[45] J.Y. Rempel, M.G. Bawendi, K.F. Jensen, J. Am. Chem. Soc. 131 (2009) 4479–4489.
[46] P.D. Cozzoli, L. Manna, M.L. Curri, S. Kudera, C. Giannini, M. Striccoli, A. Agostiano, Chemistry 17 (2005) 1296–1306.
[47] F. Huang, J.F. Banfield, J. Am. Chem. Soc. 127 (2005) 4523–4529.
[48] A.S. Michaels, A.R. Colville, J. Phys. Chem. 64 (1960) 13–19.